

# Sensitivity of Indian summer monsoon rainfall forecast skill of CFSv2 model to initial conditions and the role of model biases

K Rajendran<sup>1,2,\*</sup>, Sajani Surendran<sup>1,2</sup>,  
Stella Jes Varghese<sup>2</sup> and Arindam Chakraborty<sup>3</sup>

<sup>1</sup> Multi-Scale Modelling Programme (MSMP), CSIR Fourth Paradigm Institute (CSIR-4PI), Bangalore, India

<sup>2</sup> Academy of Scientific and Innovative Research (AcSIR), Ghaziabad, India

<sup>3</sup> Indian Institute of Science (IISc), Bangalore, India

January 20, 2021

---

\* Corresponding author address: Dr. K. Rajendran, Multi-Scale Modelling Programme (MSMP), CSIR Fourth Paradigm Institute (CSIR-4PI), CSIR-NAL Belur, Wind Tunnel Road, Bangalore, 560 037. E-mail: rajend@csir4pi.in

## Abstract

This study analyses Indian summer monsoon (ISM) seasonal reforecasts by CFSv2 model, initiated from January (4-month lead time, L4) through May (0-month lead time, L0) initial conditions (ICs), to examine the cause for highest all-India ISM rainfall (ISMR) forecast skill with February (3-month lead time, L3) ICs. The reported highest forecast skill for L3 ICs is based on correlation between observed and predicted interannual variation (IAV) of ISMR. Other skill scores such as mean error, bias, RMSE, mean, standard deviation and coefficient of variation, indicate higher or comparable skill for April (L1)/May (L0) ICs. Although theory suggests that skill degrades with increase in lead-time, CFSv2 shows highest skill with L3 ICs, due to predicting ISMR excess of 1983 for which other ICs fail. But, this correct forecasting is caused by wrong forecast of La Niña, cooling of the equatorial central Pacific (NINO3.4) during the monsoon season, by L3 ICs. In observation, near-normal sea surface temperatures (SSTs) prevailed over NINO3.4 and ISMR excess was due to variation of convection over equatorial Indian Ocean or EQUINOO which CFSv2 failed to capture with all ICs. Major results are reaffirmed by analysing an optimum number of experimental reforecasts by current version of CFSv2 initiated from five late-April/early-May ICs having shorter yet useful forecast lead time. These experimental reforecasts are found to have least seasonal biases and highest correlation skill score if 1983 is excluded. Model deficiencies such as over-sensitivity of ISMR to SST variation over NINO3.4 (ENSO) and unrealistic influence of ENSO on the EQUINOO, contribute to errors in ISMR forecasting. Whereas, in observation, ISMR is influenced by both ENSO and EQUINOO. The forecast skill for Boreal summer ENSO is found to be deficient in CFSv2 with the skill being the lowest for L3/L4 ICs, hinting the possible influence of dynamical drift induced by long forecast lead-time. Rainfall occurrence despite strong cold bias over NINO3.4 in CFSv2, is associated with a stronger ocean-atmosphere coupling, with a shift of the SST-rainfall relationship pattern to slightly colder SSTs than the observed. These results warrant the need for minimisation of biases in SST boundary forcing to achieve improved ISMR forecasts.

**Keywords:** Indian Summer Monsoon Rainfall, Seasonal Reforecasts, Forecast Skill, Model Biases, ENSO, EQUINOO

# 1 Introduction

Rainfall received over India during the summer season (June to September, JJAS) is termed as the Indian summer monsoon rainfall (ISMR). There has been considerable year to year variation (known as interannual variation or IAV) in the quantum of ISMR that has a profound effect on the agricultural sector and the socioeconomic well-being of India. Hence, it is essential to predict ISMR or its departure in a season correctly to facilitate effective planning of agricultural and economic strategies, and water and hydel power management. Despite the challenges in modelling Indian summer monsoon due to its complex features and multiple processes involved, coupled ocean-atmosphere general circulation models (CGCMs) have become an essential tool for dynamical seasonal prediction. The climate forecast system version 2 (CFSv2) model of the National Centers for Environmental Prediction (NCEP), USA, is an outcome of such efforts in recent years to improve dynamical prediction and its forecast skill is widely studied (Saha et al. 2010, Krishnamurthy and Rai 2011, Pattanaik et al. 2012, Saha et al. 2014 etc.). Recently, this model is adopted by Ministry of Earth Sciences, Government of India, for dynamical seasonal prediction of Indian summer monsoon.

Over the tropics, the existence of slowly varying boundary conditions constitutes the basic premise of seasonal prediction (Charney and Shukla 1981). Anomalous IAV of sea surface temperature (SST) over the equatorial central Pacific associated with El Niño-Southern Oscillation (ENSO, Rasmusson and Carpenter 1983), is considered to be the primary source of predictability (Shukla and Wallace 1983). Krishnamurthy and Shukla (2011) examined the predictability of ISMR in eight CGCMs including CFS for forecast and predictability errors and estimated the doubling time of errors for rainfall over India, to be 4-14 days in the CFS against 4-7 days in other models. Forecast skill is to get better as the initial conditions (ICs) get closer to the prediction period and thus the highest forecast skill is expected for ICs with 0-month lead-time (L0). In other words, the skill is expected to increase (decrease) with decreasing (increasing) lead-time when considering the development of dynamical shift in model with time (Slingo and Palmer 2011) and systematic biases caused due to deficient representation of physical processes in the model. Kumar et al. (2011) analysed CFS forecast skill of monthly mean SST and precipitation and showed that the skill rapidly decays with lead time. After a lead-time of about 30-40 days, the forecast

skill for monthly mean was found to deteriorate, with the SST anomalies in the tropical central/eastern Pacific playing a dominant role. Thus, for seasonal predictability, the conditions of the ocean state also become very important. They suggested the reduction in skill is due to the large contribution from the atmospheric internal variability to monthly means.

Contrary to expectation and the understanding of significant ENSO spring predictability barrier and low predictability of ENSO forecasts during February-March (Webster and Yang 1992), CFSv2 predictions of ISMR with February ICs (3-month lead time, L3), are reported to have the maximum forecast skill (Pokhrel et al. 2016, Ramu et al. 2016, Pillai et al. 2018, Rao et al. 2019), based on the correlation between observed and predicted IAV of ISMR during the analysis period. Further, the skill scores reported in previous studies vary considerably among themselves depending upon i) the region selected for averaging the summer season rainfall to estimate ISMR for each year, ii) the reference dataset used as observation and iii) the duration of the analysis period. These seasonal forecast verifications are performed with datasets rarely exceeding 29 samples, which can also lead to highly uncertain scores (Schaeysbroeck and Vannitsem 2019). However, an understanding of the impact of different ICs on ISMR forecast skill is fundamental and central to improving its predictability. Thus, it is imperative to understand what contributes to the forecast skill of February (L3) ICs. We focus on the factors which influence ISMR variability in CFSv2 by comparing its seasonal reforecasts (hindcasts) with observations/reanalyses, with emphasis on its dependence on SST boundary forcing. We analysed large datasets of 124 CFSv2 reforecasts initialised with ICs from 1<sup>st</sup> January to 31<sup>st</sup> May, which are made available by NCEP. To reconfirm major results and to understand the advantage of choosing ICs which are nearer to the forecast period (JJAS) yet having useful lead-time, we assessed the performance skill of the current version of CFSv2 by analysing its reforecasts initialised with an optimum subset of 5 late-April/early-May ICs.

## **2 Model, reforecasts, datasets and methodology**

CFSv2 is a coupled dynamical forecast system with Global Forecast System model in triangular truncation of T126 ( $\sim 0.9375^\circ$  horizontal resolution) with 64 hybrid sigma-pressure levels as the atmospheric component and Geophysical Fluid Dynamics Laboratory Modular Ocean Model v.4 (GFDL MOM4)

with  $0.25^\circ$  horizontal resolution in equatorial region ( $\pm 10^\circ$  latitude and  $0.5^\circ$  elsewhere) as the ocean component (Saha et al. 2014).

To examine the dependence of ISMR forecast skill of CFSv2 on ICs, we have analysed 124 nine-month retrospective seasonal reforecasts or hindcasts (hereafter referred to as 'CFSv2-NCEP') initiated from CFS Reanalysis based ICs on every 5<sup>th</sup> day starting from 1<sup>st</sup> January (4-month forecast lead time, 'L4') to 31<sup>st</sup> May (0-month lead time, 'L0'), with four reforecasts per day (at 00, 06, 12, 18 UTC) during 1982-2010 period (Saha et al. 2010). These datasets are made available by NCEP in their web portal (<https://www.ncdc.noaa.gov/data-access/model-data/model-datasets/climate-forecast-system-version2-cfsv2>). Thus, CFSv2-NCEP seasonal reforecasts initiated with 28 L4 ICs, 20 L3 ICs, 24 L2 ICs, 24 L1 ICs and 28 L0 ICs, during 1982-2010, are analysed.

We have carried out a set of nine-month reforecasts for the analysis period, with short lead times of late-April (L1) ICs (00UTC of 21 April and 26 April) and early-May (L0) ICs (00UTC of 1 May, 6 May and 11 May), using the current version of CFSv2 (which is being used for seasonal prediction as monsoon mission model by MoES, India), at the computing platform of Council for Scientific and Industrial Research (CSIR) Fourth Paradigm Institute, Bangalore (hereafter referred to as 'CFSv2-CSIR'). Our analysis of retrospective forecasts revealed that the bias in representing the spatial distribution of climatological mean Indian summer monsoon rainfall is reduced with May ICs. The skill scores of correlation between the observed and predicted IAV of ISMR during 1982-2010, are also found to be better for the ensemble means of April and May ICs, which are comparable to February ICs. This led us to choose an optimum subset of 5 late-April/early-May ICs which are close to the onset of the monsoon season yet having reasonable and useful lead time at the same time yielding good skill scores in forecasting interannual variability of ISMR. For performing a set of experimental reforecasts which creates large outputs for about 3 decades, we have optimised the number of ICs to 5 which can yield the best skill score, i.e., two late-April and three early May ICs. These runs are analysed to verify major results on forecast skill for ISMR and summer-time ENSO, in the current version of the model. In addition, for the special year of 1983, we have carried out CFSv2-CSIR reforecasts with February (L3) ICs as well.

For validation,  $0.25^\circ \times 0.25^\circ$  gridded India Meteorological Department (IMD) rainfall (Pai et al.

2014), Global Precipitation Climatology Project (GPCP) version 2.3 data (Adler et al. 2003) and Hadley Centre Ice and SST (HadISST) data (Rayner et al. 2003) are used. Daily optimum interpolation SST version 2.1 (OISSTv2.1 at  $0.25^\circ \times 0.25^\circ$  horizontal resolution) data (Reynolds et al. 2007) is also analysed. For validation of 850 hPa winds, we use 5<sup>th</sup> generation European Centre for Medium Range Weather Forecast Reanalysis (ERA5) data (Hersbach et al. 2020). NINO3.4 ( $170^\circ$ - $120^\circ$ W;  $5^\circ$ S- $5^\circ$ N) SST anomaly (normalised by standard deviation) is used as ENSO index. ENSO index  $> 1$  ( $< 1$ ) indicates El Niño (La Niña). It is important to note that our analysis focuses on ENSO during the Indian summer monsoon season (i.e. JJAS). Negative of the anomaly of surface zonal wind at the equatorial Indian Ocean (IO,  $60^\circ$ - $90^\circ$ E;  $2.5^\circ$ S- $2.5^\circ$ N) estimated from ERA5 is used as the index for equatorial Indian Ocean oscillation (EQUINOO, Gadgil et al. 2004).

For estimating seasonal mean ISMR for each year, we use the rainfall averaged over the monsoon region (Gadgil et al. 2019). Anomalies of ISMR, and indices of ENSO and EQUINOO are standardised with their standard deviation. For assessing the performance of forecasting the IAV of ISMR, basic skill scores such as ISMR temporal mean, standard deviation and coefficient of variation (CV) are used. Deterministic skill scores such as mean error, bias and root-mean-square error (RMSE) are also used. Details of these methods are provided in Appendix 1. To assess climatological mean monsoon rainfall pattern over India, statistics with respect to IMD rainfall viz. spatial pattern correlation coefficient (PCC), ratio of standard deviation against observed (SD) and climatological bias as percentage of observed (bias), are computed.

### 3 Dependence of ISMR forecast skill on initial conditions

Figure 1a shows the interannual variation (IAV) of standardised ISMR anomalies from IMD observation and deterministic ensemble mean of CFSv2-NCEP L3 reforecasts. The correlations for deterministic reforecasts against the observed for 1982-2010 period ( $\gamma$ ) for CFSv2-NCEP reforecasts with L0 to L4 ICs are written in Fig. 1a. It can be seen that the ISMR forecast skill based on correlation is the highest for CFSv2-NCEP L3 ( $\gamma=0.44$ ) followed by CFSv2-NCEP April (L1) ICs ( $\gamma=0.35$ ). We can see that the performance of ensemble mean of CFSv2-CSIR reforecasts with late-April/early-May ICs (Fig. 1a) is

comparable with that of L3 ( $\gamma=0.38$ ).

Corresponding IAV of Boreal summer ENSO index (NINO3.4 SST) anomalies is shown in Fig. 1b. ISMR excess of 1983 in L3 is associated with erroneous Boreal summer (JJAS) La Niña forecast when the observed SST condition was neutral over NINO3.4 (Fig. 1b). The extreme ISMR departure in 1983 is captured only by February ICs, in magnitude and sign. To some extent, the departure of 1994 is also captured by CFSv2-NCEP L3. However, all ICs fail to forecast the departures of 1985, 1990, 1997, 1998 and 2006. For these special years, departures of ISMR and ENSO index predicted by the ensemble means of CFSv2-NCEP reforecasts with L4 to L0 ICs are compared in Table 1. We can see that the ISMR departures in CFSv2-NCEP are largely influenced by the sign and magnitude of their ENSO index forecasts; ISMR deficits are associated with El Niño or the anomalous warming of NINO3.4 SST and excesses are associated with La Niña or the anomalous cooling of SSTs over NINO3.4 region. The inverse relationship and interaction between ENSO and ISMR during boreal summer, are well-documented (Walker and Bliss 1932, Walker 1933, Sikka 1980, Torrence and Webster 1999 etc.). This relationship is modulated on decadal timescales (Kumar et al. 1999, Chen et al. 2010, Kumar et al. 2006, Azad and Rajeevan 2016, Fan et al. 2017). Most importantly, in CFSv2-NCEP reforecasts, ISMR is shown to be having over-sensitivity to ENSO, especially to the SST fluctuation over the equatorial central Pacific region (Vishnu et al. 2019).

Further examination of yearly ISMR departures, reveals that skill is not better in CFSv2-NCEP L3 compared to CFSv2-CSIR (Fig. 1a), though their correlations are 0.44 and 0.38 respectively. The difference between these two correlations is significant only at 0.73% confidence level. However, the previous studies (Pokhrel et al. 2016, Ramu et al. 2016, Pillai et al. 2018, Rao et al. 2019) have all reported the skill improvement in CFSv2 with February ICs with such differences in correlations, though the exact correlation values vary from one study to another depending upon the region selected to compute average seasonal ISMR, the data used as reference/observation and the duration of the analysis period.

In observation, the ISMR departures of 1983, 1994, 1985, 1990, 1997, 1998 and 2006 are not strongly (and inversely) related to ENSO anomalies (Table 1). The excesses of 1983 and 1990 are associated with neutral ENSO phases and excesses of 1994 and 2006 are associated with mild warming and deficit of

1985 is associated with strong cooling over NINO3.4. In spite of strong El Niño in 1997 and La Niña in 1998, the ISMR remained close to normal in observation. In comparison, ISMR departures of 1985, 1990, 1997, 1998 and 2006, are associated with very intense NINO3.4 SST anomalies in the model and all ICs forecast the inverse ISMR departures. During these years the inverse relationship is strong and evident in the model and the dominant driving force determining the ISMR departure remains to be ENSO with all ICs. Compared to observation, the model tends to show amplified ENSO anomalies (skewed for cold events), more for earlier ICs of L4-L2 and most conspicuously for L3. For 1983 and 1994, larger errors are seen in ENSO predictions, with the largest error amplitudes for L3.

It can be seen that the correlation for CFSv2-NCEP L3 falls to 0.4 which is lower than the corresponding score ( $\gamma=0.42$ ) for CFSv2-CSIR, if we exclude 1983 (Fig. 2). So the improved ISMR forecast skill of L3 is contributed by its prediction of 1983 ISMR excess. Next, we applied other deterministic verification scores such as the mean error, bias, and RMSE during the analysis period, for assessing the forecast skill of CFSv2-NCEP L3 and CFSv2-CSIR (Table 2). These skill scores are clearly improved in CFSv2-CSIR reforecasts compared to CFSv2-NCEP L3 (Table 2). The deficiencies of underestimation of the mean (dry bias) and standard deviation (reduced variability) of ISMR, also get improved and CV becomes the closest to the observed in CFSv2-CSIR.

Model intercomparison studies in the past had suggested that models which are skilful in representing climatological mean summer monsoon rainfall are more adept in simulating IAV of ISMR (Sperber and Palmer 1996, Gadgil and Sajani 1998). CFSv2 is found to have reasonable skill in capturing the spatial distribution of climatological JJAS mean rainfall, SST and 850 hPa winds over Indian region. The mean bias is lower in CFSv2-CSIR than in L3 (Fig. 3). Still, there exists underestimation of rainfall (dry bias) over central India coinciding the seasonal monsoon trough zone, and uniform wet bias and widespread underestimation of SST (cold bias) over the Indian Ocean and West Pacific. Oceanic regions with enhanced rainfall are associated with convergence and colder SSTs. Wet bias over equatorial IO has zonal asymmetry with the maximum over the eastern equatorial Indian Ocean (EEIO) with strong westerly wind biases and low-level convergence. Cold bias over the equatorial central Pacific is found to be associated with the strengthening of ITCZ (wet bias) and with cyclonic wind bias slightly north of

equator (not shown).

Dry bias over India is larger in CFSv2-NCEP L3 compared to CFSv2-CSIR. The pattern correlation coefficient (PCC), standard deviation (SD) and mean bias are largely comparable among ensemble means of CFSv2-NCEP and CFSv2-CSIR reforecasts (Table 3). But, the PCC is slightly larger for reforecasts with May ICs. Similarly, standard deviation and bias are clearly improved in CFSv2-CSIR reforecasts with late-April/early-May ICs and it is better than L3 in representing mean monsoon rainfall over the Indian region. This is expected as atmospheric and oceanic states are close to JJAS. The increase in bias as lead-time increases, indicates the role of dynamical drift in the model.

### **3.1 ISMR-ENSO relationship**

The leading factor determining IAV of ISMR is the strong relationship between ISMR and ENSO in which there is an increased propensity of droughts during El Niño and of excess rainfall during La Niña (Sikka 1980). It can be gleaned from Fig. 1 that 8 out of 12 excess events are associated with La Niña and 8 out of 12 deficit events are associated with El Niño in CFSv2-NCEP L3. There are no large excess (large deficit) associated with El Niño (La Niña). All large excesses (large deficits) are associated with La Niña (El Niño). Thus, ISMR-ENSO relationship is much stronger in CFSv2-NCEP L3 with a correlation of -0.85 than in observation ( $\gamma=-0.44$ ) where other factors do influence ISMR (Fig. 4). The strongest correlation is seen for L4 followed by L3 and the correlation is the lowest for L0 ICs. For CFSv2-CSIR reforecasts with late-April/early-May ICs, the correlation is -0.79 which is closer to the observation compared to L3. It is to be recalled that its ISMR forecast skill is also comparable with L3 for 1982-2010 period which becomes better ( $\gamma=0.42$ ) than that of L3 ( $\gamma=0.40$ ) when 1983 is excluded from the analysis period (Fig. 2). Thus, the correct forecast of 1983 ISMR excess as a result of an erroneous La Niña forecast by L3 contributed to the seemingly higher IAV correlation for L3. But, other skill scores do not show higher ISMR forecast skill for L3 (Table 2). Moreover, the Boreal summer ENSO forecast skill is the lowest for L3 (Fig. 1b). This makes it necessary to analyse its ENSO forecast skill during Boreal summer, in detail.

### *Boreal summer ENSO forecast skill*

CFSv2-NCEP L3 appears to have serious deficiency in forecasting summer-time ENSO (Fig. 1b). The forecast skill for JJAS ENSO index is found to be the lowest in CFSv2-NCEP L3 and L4 ( $\gamma=0.59$ ) compared to those in L2 to L0, and in CFSv2-CSIR ( $\gamma=0.76$ ). We have seen that the skill is much higher when all 124 reforecasts are considered together with the correlation of their median with the observed being 0.74 (not shown). The verification of performance of CFSv2 in predicting the warm and cold SST anomalies over the NINO3.4 region can be done from the classification of hits, misses and false alarms in CFSv2-NCSP L3 and CFSv2-CSIR reforecasts (Table 4). The forecasts miss several events and there are a few false alarms as well. The number of misses and false alarms for cold and warm events is more for L3 forecasts. Thus, the performance is slightly better for CFSv2-CSIR reforecasts with late-April/early-May ICs.

Monthly forecast skill scores for ENSO indices against the observed during the analysis period (written in Figs. 5a-d) clearly manifest the bias in L3 ENSO forecasts for June, July, August and September. During 1983, L3 predicted neutral condition in June and thereafter strong La Niña which kept intensifying from July to September. In contrast, in observation, NINO3.4 was having El Niño in June, neutral conditions in July and August, and a mild cold anomaly in September. The forecast skill for 1982-2010 period, systematically drops from June to September with the least skill exhibited in September (Fig. 5).

Correspondingly, the relationship of NINO3.4 SST with local NINO3.4 rainfall and remote impact on ISMR in 1983, show model biases in L3. In observation, there is enhanced NINO3.4 rainfall associated with El Niño in June which tends to become normal as SSTs approach climatology and then develops to a cold anomaly by September. Accordingly, ISMR varies from below normal in June to normal in July to large excesses in August and September. This is consistent with the inverse relationship between ISMR and ENSO. In L3, ENSO condition is near-neutral with excess rainfall over NINO3.4 in June which drops to strong La Niña in July which intensifies thereafter with deficit rainfall over NINO3.4. This results in above-normal ISMR in June and large excesses in July to September of 1983.

The strong association of local rainfall with NINO3.4 SST, even with cold bias over the equatorial Pacific Ocean in CFSv2 (not shown), can be understood from the SST-rainfall relationship over NINO3.4

from June to September of 1982-2010 (Fig. 6). Figure 6 shows the number of points for each 0.25°C SST and 0.5 mm/day rainfall bin, along with the variation of mean rainfall with SST. The observed relationship ( $\gamma=0.59$ ) shows that the rainfall along with the mean steadily increases with SST from about 27°C with high propensity of rainfall for SSTs above this threshold. In CFSv2-NCEP L3, there is a slight shift in the SST-rainfall relationship towards colder SSTs (Fig. 6) with the number of observations above 28°C becoming much lower than the observed. This is consistent with the finding that the SST-rainfall pattern in coupled models is similar to the corresponding observation or atmosphere-only version, except for a shift of the pattern to colder/warmer SSTs as per their seasonal mean cold/warm bias (Rajendran et al. 2012).

## **4 Role of bias in SST boundary forcing**

In CFSv2, the SST-rainfall association/relationship over NINO3.4 is stronger with a correlation of 0.65 than observed (Fig. 6), which in turn seems to have a remote impact on ISMR. Thus the ISMR prediction depends highly on ENSO. This indirectly implies that the reduction of SST bias over central Pacific can contribute to improvement in ISMR forecast skill. Further, daily SST averaged over the NINO3.4 region shows that SST starts falling sharply after the beginning of monsoon season in 1983 (Fig. 7). The dropping of SST is steep and large. The characteristics of the evolution of 1983 SST over NINO3.4 for L3 ICs remain the same in the current version of CFSv2 as well (i.e., CFSv2-CSIR initiated with February ICs). The build-up of bias hints at the role of dynamic drift and model bias resulting in colder SSTs by the summer months for L3. Given the high sensitivity of ISMR to NINO3.4 SST boundary forcing, systematic approach to minimise SST bias is essential to achieve the potential predictability.

### **4.1 Link of ISMR with Equatorial Indian Ocean**

Another mode of SST variability in the equatorial Indian Ocean (IO), is the occurrence of opposite SST anomalies over eastern equatorial IO (EEIO, 90°-110°E; 10°S-0°) and western equatorial IO (WEIO, 50°-70°E; 10°S-10°N), known as the Indian Ocean dipole (IOD, Saji et al. 1999). Climatologically, IO is warmer in the east supporting more convection than in the west during monsoon. Positive IOD phase is characterized by weakening or reversal of climatological zonal SST gradient with suppression

(enhancement) of convection over east (west) and anomalous winds blow from east to west along the equator, lifting up of thermocline and mixed layer of the east. However, the relationship between ISMR and IOD during JJAS is found to be rather weak, with the correlation coefficient not significantly different from zero, and only about 1% of ISMR variance explained by IOD (Sajani et al. 2015).

The atmospheric counterpart of IOD, the equatorial Indian Ocean Oscillation (EQUINOO), with its positive (negative) phase associated with enhanced convection over WEIO (EEIO) and suppressed convection over EEIO (WEIO) is found to play an important role in determining IAV of ISMR (Gadgil et al. 2004) with the positive (negative) phase favourable (unfavourable) for ISMR. As the positive (negative) EQUINOO phase is associated with an easterly (westerly) anomaly of the zonal wind over the central equatorial IO, the EQUINOO index is based on the surface zonal wind anomaly over this region. Although EQUINOO is considered to be the atmospheric component of the coupled IOD mode, unlike ENSO, they are not as tightly coupled (Sajani et al. 2015) with correlation between their indices being only  $\sim 0.45$ .

Spatial distribution of 1983 anomalies of rainfall, SST and winds show that in observation, the enhanced rainfall over India is due to a positive EQUINOO (convective WEIO), whereas, in CFSv2-NCEP L3, it is associated with La Niña (Figs. 8a and b). In CFSv2-CSIR, ISMR deficit is associated with El Niño (Fig. 8c). Both forecasts do not show the important positive association between monsoon rainfall over WEIO and Indian region. Further analysis reveals that in CFSv2, EQUINOO appears to occur due to the impact of ENSO on the equatorial Indian Ocean. The impact of El Niño results in warming and enhancement of rainfall over WEIO and cooling and suppression of rainfall over EEIO region extending up to the West Pacific and over the Indian region. During La Niña opposite impacts occur over WEIO, EEIO and Indian region. Thus, ENSO elicits an inverse relationship between WEIO and EEIO which is analogous to the EQUINOO characteristics over the Indian Ocean. At the same time, ENSO impact results in an inverse relationship between ISMR and WEIO rainfall which is in contrast to their observed relationship associated with EQUINOO. The fact that enhanced cross-equatorial flow is associated with enhanced off-equatorial diabatic heating along the monsoon convergence zone over India results in a strong positive correlation between convection over WEIO and ISMR which is observed during strong

EQUINOO events. But, this relationship fails to exist in CFSv2. In contrast, ‘EQUINOO-like’ events with opposite poles of anomalies of SST, rainfall and circulation over equatorial WEIO and EEIO occur which are induced by ENSO in the model (not shown). This endorses opposite relationship between WEIO convection and ISMR.

In CFSv2, ENSO and EQUINOO result in reinforcing each other’s inverse impact on ISMR, in contrast to observation where they tend to oppose each other (Vishnu et al. 2019). This leads to much stronger than the observed inverse relationship between ENSO and ISMR in CFSv2 (Fig. 4). Correspondingly, ENSO and EQUINOO show an intense correlation between them; 0.83 in CFSv2-NCEP L3 (largest among ICs) and 0.58 in CFSv2-CSIR. In contrast, in observation they are almost independent ( $\gamma=0.14$ , Fig. 9a). Resultantly, ISMR-EQUINOO relationship is also too strong in CFSv2-NCEP L3 ( $\gamma=-0.77$ , the largest among ICs,  $\gamma=-0.56$  for CFSv2-CSIR) which is opposite to the observed ( $\gamma=0.54$ ) relationship (Fig. 9b).

Forecast of 1994 ISMR departure by L3 was also due to an erroneous La Niña forecast when in reality ISMR was excess only due to positive EQUINOO (coloured as green for positive EQUINOO and red for negative EQUINOO events in Table 1). In CFSv2, ISMR departure is almost entirely decided by ENSO whereas in observation EQUINOO is found to play a decisive role in several years (Table 1). It can be seen that excesses of 1983 (with neutral ENSO condition) and 1994 and 2006 (with mild warm ENSO anomalies) are due to positive EQUINOO events. ISMR of 1985 was below normal due to negative EQUINOO despite having very strong cold ENSO anomaly. Normal monsoons of 1997 and 1998 are due to positive and negative EQUINOO events despite having very strong El Niño and La Niña respectively. Inability of CFSv2 to forecast EQUINOO events independent of ENSO, made it impossible for the model to forecast ISMR anomalies of 1985, 1990, 1997, 1998 and 2006 with almost all ICs (Figs. 1a and Table 1).

## 5 Concluding Remarks

This study attempts to understand what contributes to the highest ISMR forecast skill for CFSv2 February (3-month forecast lead time, L3) ICs as reported in previous studies. We analysed 124 retrospective

nine-month reforecasts by CFSv2 with January (4-month forecast lead time, L4) through May (0-month forecast lead time, L0) ICs, provided by NCEP for 1982-2010 period (referred to as CFSv2-NCEP reforecasts). Our analysis reveals that the reported higher forecast skill for February (L3) ICs was based on a single skill score of correlation between observed and predicted ISMR departures during the analysis period. In contrast, other skill scores such as the mean error, interannual bias and RMSE, and the mean, standard deviation and coefficient of variation, indicate higher or comparable forecast skill for April/May (L1/L0) ICs. Climatological bias in mean summer monsoon rainfall over India is also found to be the least with L1/L0 ICs. These results are reconfirmed through the analysis of a set of experimental reforecasts by the current version of CFSv2 with an optimum subset of 5 late-April/early-May ICs which are having shorter yet useful forecast lead times (referred to as CFSv2-CSIR reforecasts). Correspondingly, reforecasts with late-April/early-May ICs yield a correlation skill score comparable to that of L3 and the deterministic ISMR forecast skill is found to be the best with late-April/early-May ICs for 1982-2010 period, if 1983 is excluded.

The success of CFSv2-NCEP L3 in forecasting a single event, i.e., excess ISMR departure in 1983, contribute to its higher IAV correlation of 0.44. The correlation is 0.38 for CFSv2-CSIR late-April/early-May ICs which is significantly different from that of CFSv2-NCEP L3 with only 73% confidence. These correlations become 0.40 and 0.42 for CFSv2-NCEP L3 and CFSv2-CSIR respectively, if 1983 is excluded from the analysis period of 1982-2010. Further, we find that the success of CFSv2-NCEP L3 in forecasting 1983 ISMR excess is due to its wrong forecast of La Niña (unlike L1 and L0 ICs) during Boreal summer of 1983. Our analysis thus suggests the importance of initialising seasonal forecasts from April/May ICs.

CFSv2's common deficiencies such as the over-intensified influence of ENSO on ISMR and on variation of SST, rainfall and circulation over the equatorial Indian Ocean, are also important factors which contribute to errors in ISMR forecasting. In CFSv2, ISMR is almost entirely decided by ENSO related SST boundary forcing, with no link between variabilities of ISMR and convection over equatorial Indian Ocean associated with EQUINOO. In contrast, in observation, ISMR is influenced by both ENSO and EQUINOO independently.

Central Pacific was under the sway of El Niño till June 1983. All forecasts were initiated when El Niño was prevailing with active convection over NINO3.4. CFSv2 is known to develop pronounced wet and cold bias over the central Pacific. The fact that CFSv2-NCEP L3 with long lead-time ended in forecasting La Niña in summer hints at the possible role of wet bias and associated winds resulting in stronger cooling of NINO3.4 ocean surface for L3. This also implies that the persistence of errors in atmospheric circulation due to imperfections in physical processes could eventually lead to large-scale bias in ocean circulation and surface temperatures. This can be manifested in larger magnitudes in forecasts with longer lead-times. Improvements in atmospheric model physics schemes and experiments with observed SST forced atmosphere-only component of CFSv2 can throw further light on these aspects. It is also important to see if the ocean model of CFSv2 can simulate oceanic modes correctly when forced with realistic atmospheric circulation and fluxes. Our analysis suggests the need for a systematic approach to minimise the biases in SST boundary forcing in CFSv2, to achieve improved ISMR forecasts.

### **Acknowledgements**

We thank Prof. JS for many useful discussions and suggestions. This study is supported by National Monsoon Mission Phase-II project (GAP-1013) funded by the Ministry of Earth Sciences (MoES), Government of India. We acknowledge the availability of CSIR-4PI HPC, Anantha. The authors acknowledge valuable discussions with Prof. Ravi S Nanjundiah of IISc on the implementation of CFSv2 on Anantha. We are thankful to the NOAA National Centers for Environmental Information and National Centers for Environmental Prediction (NCEP) which is responsible for Climate Forecast System (CFS), for making available the CFSv2 reforecasts' outputs (Saha et al. 2014) on their web portal ([https://www.ncdc.noaa.gov/data-access/model-data/model-datasets/climate-forecast-system-version2 - cfsv2](https://www.ncdc.noaa.gov/data-access/model-data/model-datasets/climate-forecast-system-version2-cfsv2)). We acknowledge the NCEP Climate Forecast System Reanalysis initial conditions (Saha et al. 2010) provided in the above portal which are used for carrying out seasonal reforecasts of CFSv2 with late-April/early-May initial conditions during 1982-2010. We also acknowledge the India Meteorological Department (IMD) for providing  $0.25^\circ \times 0.25^\circ$  gridded rainfall ([http://imdpune.gov.in/Clim\\_Pred\\_LRF\\_New/Gridded\\_Data\\_Download.html](http://imdpune.gov.in/Clim_Pred_LRF_New/Gridded_Data_Download.html), Pai et al. 2014), Global Precipitation Climatology Project (GPCP) version 2.3 data (<https://psl.noaa.gov/data/gridded/data.gpcp.html>, Adler et al. 2003), Hadley Centre Ice and

SST (HadISST) data ([http://badc.nerc.ac.uk/view/badc.nerc.ac.uk\\_\\_ATOM\\_\\_dataent\\_hadisst](http://badc.nerc.ac.uk/view/badc.nerc.ac.uk__ATOM__dataent_hadisst), Rayner et al. 2003), 5<sup>th</sup> generation European Centre for Medium Range Weather Forecast Reanalysis (ERA5) data (<https://www.ecmwf.int/en/forecasts/datasets/reanalysis-datasets/era5>, Hersbach et al. 2020) and NOAA High Resolution SST data provided by the NOAA/ OAR/ESRL PSL, Boulder, Colorado, USA, at their Web site at <https://psl.noaa.gov/> (Reynolds et al. 2007).

## References

1. Adler, R. F., Huffman, G. J. Chang, A. and co-authors, The version 2 Global Precipitation Climatology Project (GPCP) monthly precipitation analysis (1979-present). 2003, *J. Hydrmeteorol.*, **4**, 1147-1167.
2. Azad, S., and Rajeevan, M., Possible shift in the ENSO-Indian monsoon rainfall relationship under future global warming. 2016, *Sci. Rep.*, **6(1)**, 20145.
3. Charney, J. G. and Shukla, J., Predictability of monsoons. 1981, *Monsoon dynamics*, **4**, 99-109.
4. Chen, W., Dong, B., and Lu, R., Impact of the Atlantic Ocean on the multidecadal fluctuation of El Niño-Southern Oscillation-South Asian monsoon relationship in a Coupled General Circulation Model. 2010, *J. Geophys. Res.*, **115**, D17109.
5. Fan, F., and co-authors, Revisiting the relationship between the south Asian summer monsoon drought and El Niño warming pattern. 2017, *Atmos. Sci. Lett.*, **18(4)**, 175-182.
6. Gadgil, Sulochana, and Sajani, Surendran, Monsoon precipitation in the AMIP runs. 1998, *Clim. Dyn.*, **14**, 659-689.
7. Gadgil, Sulochana., Vinayachandran, P. N., Francis, P. A., and Gadgil, S., Extremes of Indian summer monsoon rainfall, ENSO, equatorial Indian Ocean oscillation. 2004, *Geophys. Res. Lett.*, **31**, L12213.
8. Gadgil, Sulochana., Rajendran, K., and Pai, D. S., A new rain-based index for the Indian summer monsoon rainfall. 2019, *Mausam*, **70(30)**, 485-500.
9. Hersbach, H., Bell, B., Barrisford, P., Hirahara, S., and co-authors, The ERA5 global reanalysis. 2020, *Quart. J. Roy. Meteorol. Soc.*, **146 (730)**, 1999-2049.
10. Krishnamurthy, V. and Rai, S., Predictability of South Asian monsoon circulation in the NCEP Climate Forecast System. 2011, *Adv. Geosci.*, **22**, 65-76.

11. Krishnamurthy, V. and Shukla, J., Predictability of the Indian monsoon in coupled general circulation models. 2011, *COLA Tech. Rep.*, **313**.
12. Kumar, A., Chen, M. and Wang, W., An analysis of prediction skill of monthly mean climate variability. 2011, *Clim. Dyn.*, **37**, 1119-1131.
13. Kumar, K. K., Rajagopalan, B., and Cane, M. A., On the weakening relationship between the Indian monsoon and ENSO. 1999, *Science*, **284(5423)**, 2156-2159.
14. Kumar, K. K., Rajagopalan, B., Hoerling, M., Bates, G., and Cane, M. A., Unraveling the mystery of Indian monsoon failure during El Niño. 2006, *Science*, **314(5796)**, 115-119.
15. Pai, D. S., Latha, S., Rajeevan, M., Sreejith, O. P., Satbhai, N. S. and Mukhopadhyay, B., Development of a new high spatial resolution ( $0.25^\circ \times 0.25^\circ$ ) long period (1901-2010) daily gridded rainfall data set over India and its comparison with existing data sets over the region. 2014, *Mausam*, **65**, 1-18.
16. Pattanaik, D. R., Mukhopadhyay, B. and Kumar, A., Monthly Forecast of Indian Southwest Monsoon Rainfall Based on NCEP's Coupled Forecast System. 2012, *Atm. Clim. Sci.*, **2(4)**, 479-491.
17. Pillai, P. A., Rao, S. A. and co-authors, Seasonal prediction skill of Indian summer monsoon rainfall in NMME models and monsoon mission CFSv2. 2018, *Int. J. Climate*, **38**, e847-e861.
18. Pokhrel, S., Saha, S. K. and co-authors, Seasonal prediction of Indian summer monsoon rainfall in NCEP CFSv2: forecast and predictability error. 2016, *Clim. Dyn.*, **46**, 2305-2326.
19. Rajendran, K., Nanjundiah, R. S., Gadgil, Sulochana, and Srinivasan, J., How good are the simulations of tropical SST-rainfall relationship by IPCC AR4 atmospheric and coupled models?. 2012, *J. Earth Syst. Sci.*, **121(3)**, 595-610.
20. Ramu, D. A. and co-authors, Indian summer monsoon rainfall simulation and prediction skill in the CFSv2 coupled model: Impact of atmospheric horizontal resolution. 2016, *J. Geophys. Res. Atmos.*, **121(5)**, 2205-2221.

21. Rao, S. A. and co-authors, MONSOON MISSION: A targeted activity to improve monsoon prediction across scales. 2019, *Bull. Amer. Meteorol. Soc.*, **100(12)**, 2509-2532.
22. Rasmusson, E. M. and Carpenter, T. H., The relationship between eastern equatorial Pacific sea surface temperatures and rainfall over India and Sri Lanka. 1983, *Mon. Wea. Rev.*, **111(3)**, 517-528.
23. Rayner, N. A., Parker, D. A. and co-authors, Global analyses of SST, sea ice and night marine air temperature since the late nineteenth century. 2003, *J. Geophys. Res. Atm.*, **108**, 4407, 10.1029/2002JD002670.
24. Reynolds, R. W., Smith, T. M., Liu, C., Chelton, D. B., Casey, K. S. and Schlax, M. G., Daily High-Resolution-Blended Analyses for Sea Surface Temperature. 2007, *J. Climate*, **20**, 5473-5496.
25. Saha, S., Moorthi, S., and co-authors, The NCEP Climate Forecast System reanalysis. *Bull. Amer. Meteorol. Soc.*, 2010, **91**, 1015-1057.
26. Saha, S., Moorthi, S., Wu, X. and co-authors, The NCEP Climate Forecast System version 2. 2014, *J. Climate*, **27**, 2185-2208.
27. Sajani, Surendran, Gadgil, Sulochana, Francis, P. A. and Rajeevan, M., Prediction of Indian rainfall during the summer monsoon season on the basis of links with equatorial Pacific and Indian Ocean climate indices. 2015, *Environ. Res. Lett.*, **10**, 094004.
28. Saji, N. H., Goswami, B. N., Vinayachandran, P. N., and Yamagata, T., A dipole in the tropical Indian Ocean. 1999, *Nature*, **401**, 360-363.
29. Schaeybroeck, B. V. and Vannitsem, S., Postprocessing of Long-Range Forecasts. 2019, *In: Statistical postprocessing of ensemble forecasts*, **Chapter 10**, 267-290.
30. Shukla, J. and Wallace, J. M., Numerical simulation of the atmospheric response to equatorial Pacific sea surface temperature anomalies. 1983, *J. Atmos. Sci.*, **40**, 1613-1630.

31. Sikka, D. R., Some aspects of the large-scale fluctuations of summer monsoon rainfall over India in relation to fluctuations in the planetary and regional scale circulation parameters. 1980, *Proc. Indian Acad. Sci. (Earth Planet. Sci.)*, **89**, 179-195.
32. Slingo, J. and Palmer, T. N., Uncertainty in weather and climate prediction. 2011, *Philos. Trans. R. Soc.*, **369**, 4751-4767.
33. Sperber, K. R., and Palmer, T. N., Interannual Tropical Rainfall Variability in General Circulation Model Simulations Associated with the Atmospheric Model Intercomparison Project. 1996, *J. Climate*, **9**, 2727-2750.
34. Torrence, C., and Webster, P. J., Interdecadal changes in the ENSO-monsoon system. 1999, *J. Climate*, **12(8)**, 2679-2690.
35. Vishnu, S., Francis, P. A., Ramakrishna, S. S. V. S., and Schenoi, S. S. C., On the relationship between the Indian summer monsoon rainfall and the EQUINOO in the CFSv2. 2019, *Clim. Dyn.*, **52**, 1263-1281.
36. Walker, G. T., and Bliss, E. W., World weather. V. 1932, *Mem. Roy. Meteorol. Soc.*, **4**, 53-84.
37. Walker, G. T., Seasonal weather and its prediction. 1933, *Nature*, **132(3343)**, 805-808.
38. Webster, P. J. and Yang, S., Monsoon and ENSO: selectively interactive systems. 1992, *Quart. J. Roy. Meteorol. Soc.*, **118**, 877-926.

## Appendix 1: Forecast Skill Scores

The methods used for verifying forecasts are the following.

1. Mean error is average error.

$$\text{Mean Error} = \frac{1}{N} \sum_{i=1}^N (F_i - O_i)$$

2. Bias is comparison of average forecast magnitude to the observed.

$$\text{BIAS} = \frac{\frac{1}{N} \sum_{i=1}^N F_i}{\frac{1}{N} \sum_{i=1}^N O_i}$$

3. RMSE is average magnitude of forecast errors and Anomaly correlation is comparison of forecast anomalies to observed.

$$\text{RMSE} = \sqrt{\frac{1}{N} \sum_{i=1}^N (F_i - O_i)^2}$$

4. In addition, the amount of climatological JJAS rainfall over the Indian land region ( $\mu$ ), the corresponding standard deviation of JJAS mean rainfall ( $\sigma$ ) and its temporal coefficient of variation (CV) in percentage for 1982-2010, are estimated as:

$$\mu = \frac{\sum_{i=1}^N \text{India Rain}_{(JJAS)_i}}{N}$$

$$\sigma = \sqrt{\frac{\sum_{i=1}^N (\text{India Rain}_{(JJAS)_i} - \mu)^2}{N}}$$

$$\text{CV} = \frac{\sigma}{\mu} \times 100$$

<b>Std. Anomalies</b>	<b>1983</b>	<b>1994</b>	<b>1985</b>	<b>1990</b>	<b>1997</b>	<b>1998</b>	<b>2006</b>
<b>IMD/HadISST</b>	1.61	1.98	-0.89	0.98	0.08	0.04	1.22
	-0.04	0.46	-0.87	0.14	2.44	-1.00	0.39
<b>January ICs</b>	0.47	0.19	0.31	-1.17	-0.80	2.76	-0.51
	-0.96	-0.42	-1.22	0.92	0.71	-2.16	0.32
<b>February ICs</b>	1.20	0.86	0.34	-1.25	-1.50	2.01	-0.99
	-1.11	-1.13	-1.12	1.58	0.89	-1.80	1.19
<b>March ICs</b>	0.71	-0.40	0.98	-0.73	-1.03	1.25	-1.08
	-0.52	-0.40	-1.17	0.67	1.02	-1.23	1.09
<b>April ICs</b>	-0.06	0.13	0.93	-0.36	-1.89	2.03	-0.63
	0.04	-0.23	-1.20	-0.01	1.81	-1.19	0.65
<b>May ICs</b>	-1.11	-0.14	1.38	-0.75	-2.07	1.81	-0.85
	0.59	0.10	-1.13	0.37	2.32	-2.05	0.92

Table 1: Standardised anomalies of ISMR and ENSO index for special years of 1983 and 1994, and 1985, 1990, 1997, 1998 and 2006, for ensemble means of CFSv2-NCEP reforecasts with January (L0) to May (L4) initial conditions (ICs). For each entity, the first and the second sub-rows are the anomalies of ISMR and ENSO index respectively. Cells are coloured in green (red) if anomaly of EQUINOO index is positive (negative) for each year.

<b>IAV Skill Scores</b>	<b>CFSv2-NCEP Feb. ICs. Ens.</b>	<b>CFSv2-CSIR Apr/May Ens.</b>	<b>Observation (IMD)</b>
Mean Error (IAV)	-3.11	-1.99	
Bias (IAV)	0.64	0.69	
RMSE (IAV)	3.14	2.12	
ISMR $\mu$ (mm/day)	3.50	4.51	6.50
ISMR $\sigma$ (mm/day)	0.51	0.66	0.76
ISMR CV (%)	14.5	10.3	11.7

Table 2: Skill scores for interannual variation (IAV) of standardized (with standard deviation) anomalies of Indian summer monsoon rainfall averaged over monsoon region (ISMR), for ensemble means of CFSv2-NCEP reforecasts with February (L3) initial conditions (ICs) and CFSv2-CSIR reforecasts with late-April/early-May ICs, with respect to corresponding IMD observation for 1982-2010. Time series statistics against the observed are mean error, bias, and RMSE are shown as skill scores. The mean ( $\mu$ ), standard deviation ( $\sigma$ ) and coefficient of variation (CV in %) of ISMR for models and IMD observation are also given.

<b>CFSv2 reforecasts</b>	<b>ICs</b>	<b>PCC</b>	<b>SD</b>	<b>bias</b>
Ensemble means of CFSv2-NCEP reforecasts with L4-L0 ICs	Jan (L4)	0.69	0.86	-33.2%
	Feb (L3)	0.69	0.85	-34.0%
	Mar (L2)	0.69	0.86	-33.2%
	Apr (L1)	0.69	0.90	-27.6%
	May (L0)	0.71	0.96	-19.6%
CFSv2-CSIR reforecasts and ensemble mean	21 Apr	0.69	0.92	-27.4%
	26 Apr	0.69	0.95	-24.3%
	01 May	0.70	0.93	-24.3%
	06 May	0.71	0.95	-21.6%
	11 May	0.70	0.95	-19.8%
	5 ICs Mean	0.70	0.94	-23.5%

Table 3: Statistics for climatological summer (JJAS) mean rainfall over India for ensemble means of CFSv2-NCEP reforecasts with January (L0) to May (L4) initial conditions (ICs) and CFSv2-CSIR reforecasts with late-April/early-May ICs and their ensemble mean with respect to corresponding IMD observation for 1982-2010 period. Statistics are spatial pattern correlation coefficient (PCC), ratio of model spatial standard deviation with the observed (SD) and bias in simulating the mean with respect to IMD observation.

Cold Events			Warm Events		
HadISST	CFSv2-NCEP	CFSv2-CSIR	HadISST	CFSv2-NCEP	CFSv2-CSIR
	1983				
1984	1984	1984	1982		
1985	1985	1985	1987	1987	
		1986		1990	
1988	1988	1988	1991		
1989		1989		1993	
	1994		1997	1997	1997
	1995	1995		2001	2001
1998	1998	1998	2002	2002	2002
1999		1999	2004	2004	2004
2000				2006	2006
		2003	2009	2009	2009
2007	2007	2007			
2010		2010			

Table 4: List of cold events (left panel) and warm events (right panel) over NINO3.4 from observation (HadISST) and CFSv2-NCEP reforecasts with February (L3) ICs and CFSv2-CSIR reforecasts with late-April/early-May ICs. Cold and warm events are defined as the standardized Boreal summer (JJAS) SST anomaly being less than -0.5 and greater than 0.5 respectively. False alarms are highlighted in green and misses are coloured in red.

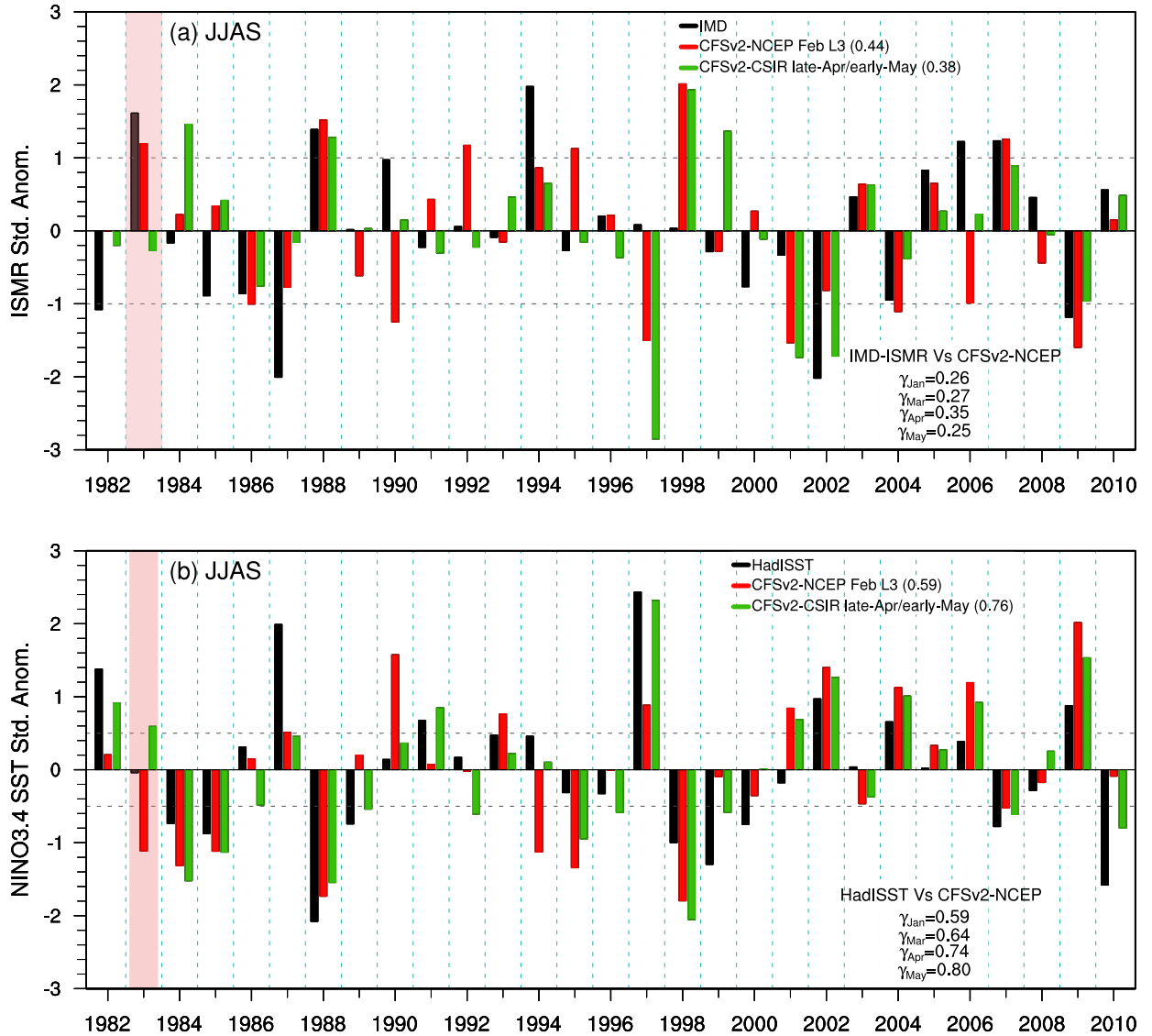


Figure 1: a) Interannual variability of standardised anomalies of Indian summer monsoon rainfall over monsoon region (ISMR) in the ensemble means of CFSv2-NCEP reforecasts with February (L3) initial conditions (ICs) and CFSv2-CSIR reforecasts with late-April/early-May ICs, are compared with the corresponding ISMR anomalies from IMD observation. Correlation coefficients ( $\gamma$ ) between observed ISMR anomalies and those from the ensemble means of CFSv2-NCEP reforecasts with L4 to L0, and CFSv2-CSIR reforecasts with late-Apr/early-May ICs, are also given. 1983 ISMR anomalies are highlighted in light red background color. b) Same as a) but for anomalies of ENSO index defined as standardised anomalies of NINO3.4 SST. Correlation coefficients between observed HadISST based ENSO index anomalies and those from the ensemble means of CFSv2-NCEP reforecasts with L4 to L0, and CFSv2-CSIR reforecasts with late-Apr/early-May ICs, are also given.

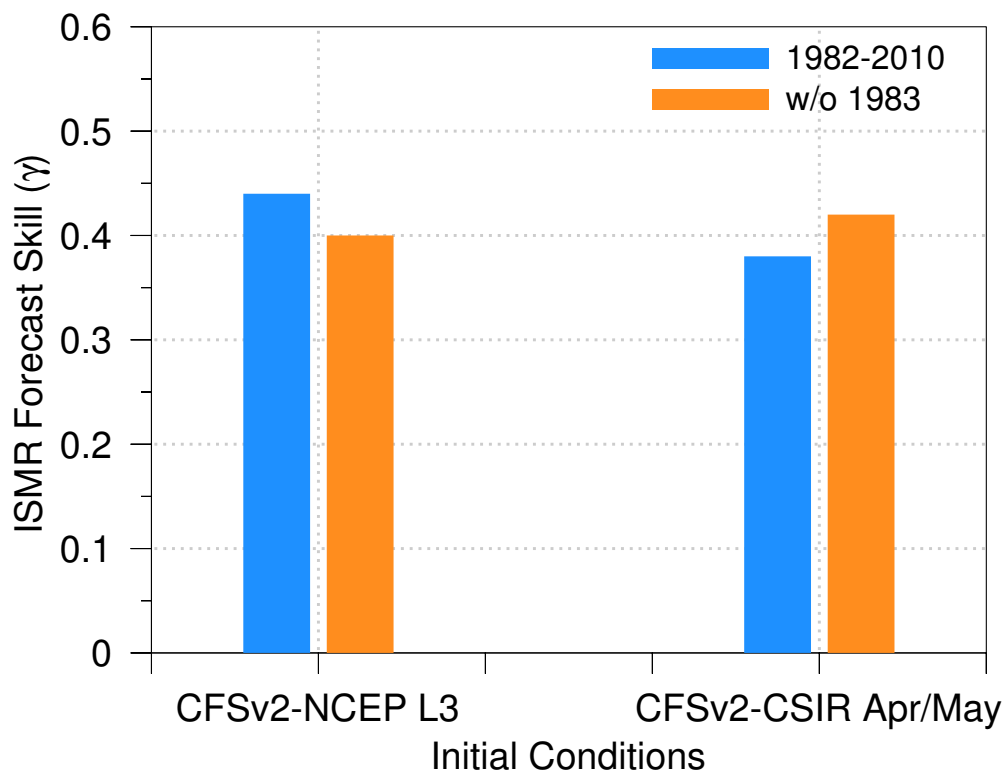


Figure 2: Correlations of standardised ISMR anomalies of deterministic (ensemble mean) CFSv2-NCEP reforecasts with February (L3) initial conditions (ICs) and CFSv2-CSIR reforecasts with late-April/early-May ICs, against the IMD based observation for i) 1982-2010 period and ii) 1982-2010 period excluding 1983.

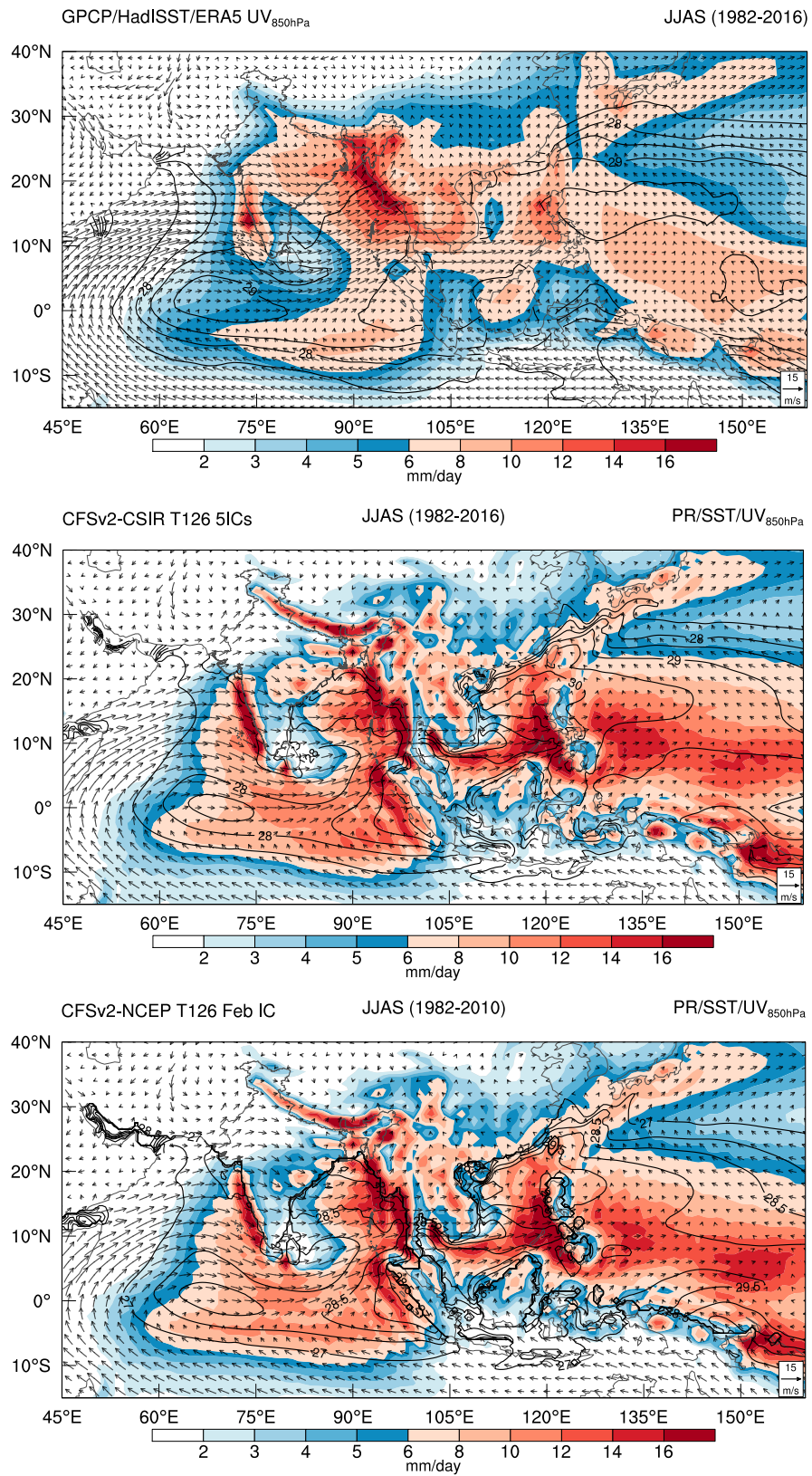


Figure 3: Climatological summer mean (JJAS) rainfall (shaded), SST (contours) and 850 hPa winds (vectors) from i) observation (top), and ensemble means of ii) CFSv2-CSIR reforecasts with late-April/early-May ICs (middle) and iii) CFSv2-NCEP reforecasts with L3 ICs (bottom).

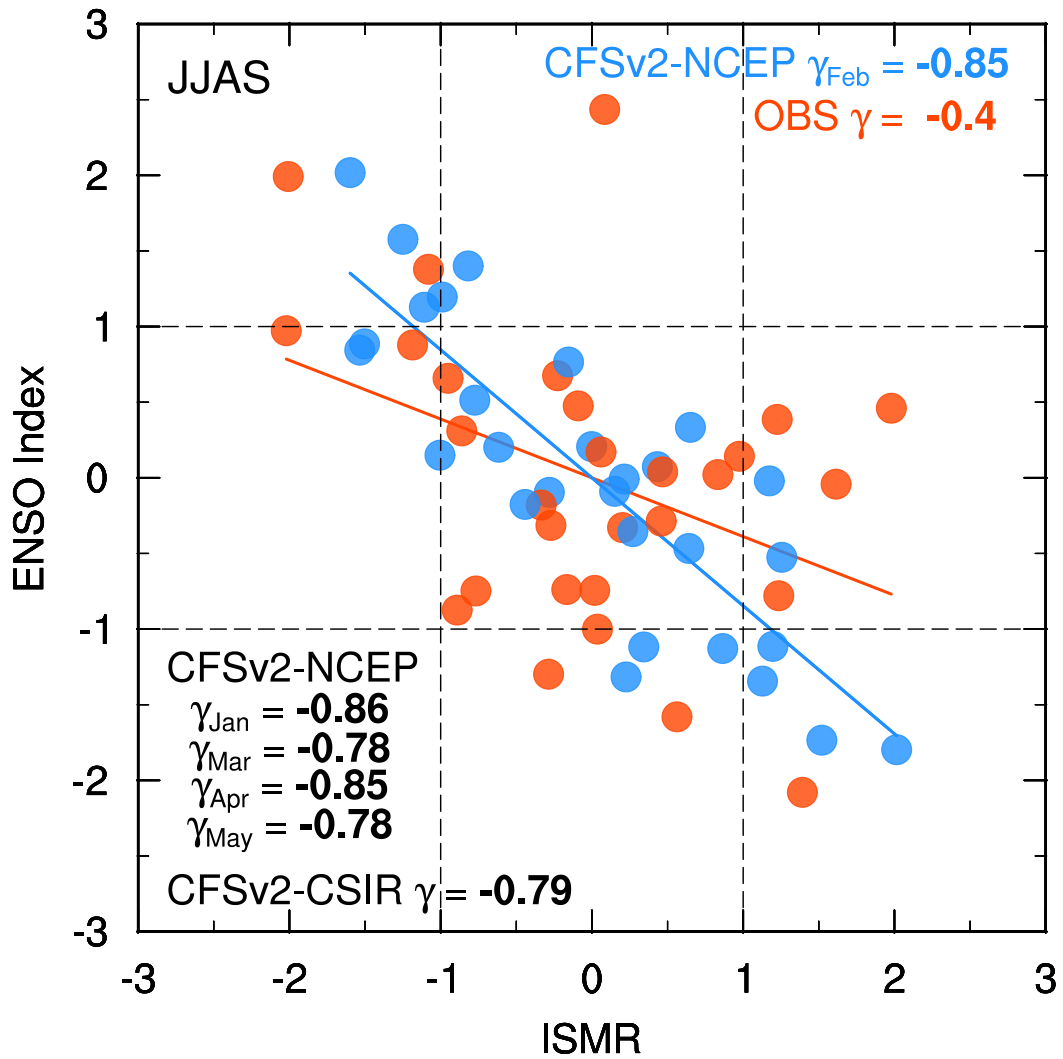


Figure 4: Anomalies of ISMR plotted against ENSO index for CFSv2-NCEP L3 (blue) and observation (red). Respective regression lines are drawn. Correlations ( $\gamma$ ) for ensemble means of CFSv2-NCEP L4, L2, L1 and L0, and CFSv2-CSIR with late-Apr/early-May ICs, are given in bottom-left corner and for CFSv2-NCEP L3 and observation are given in top-right corner.

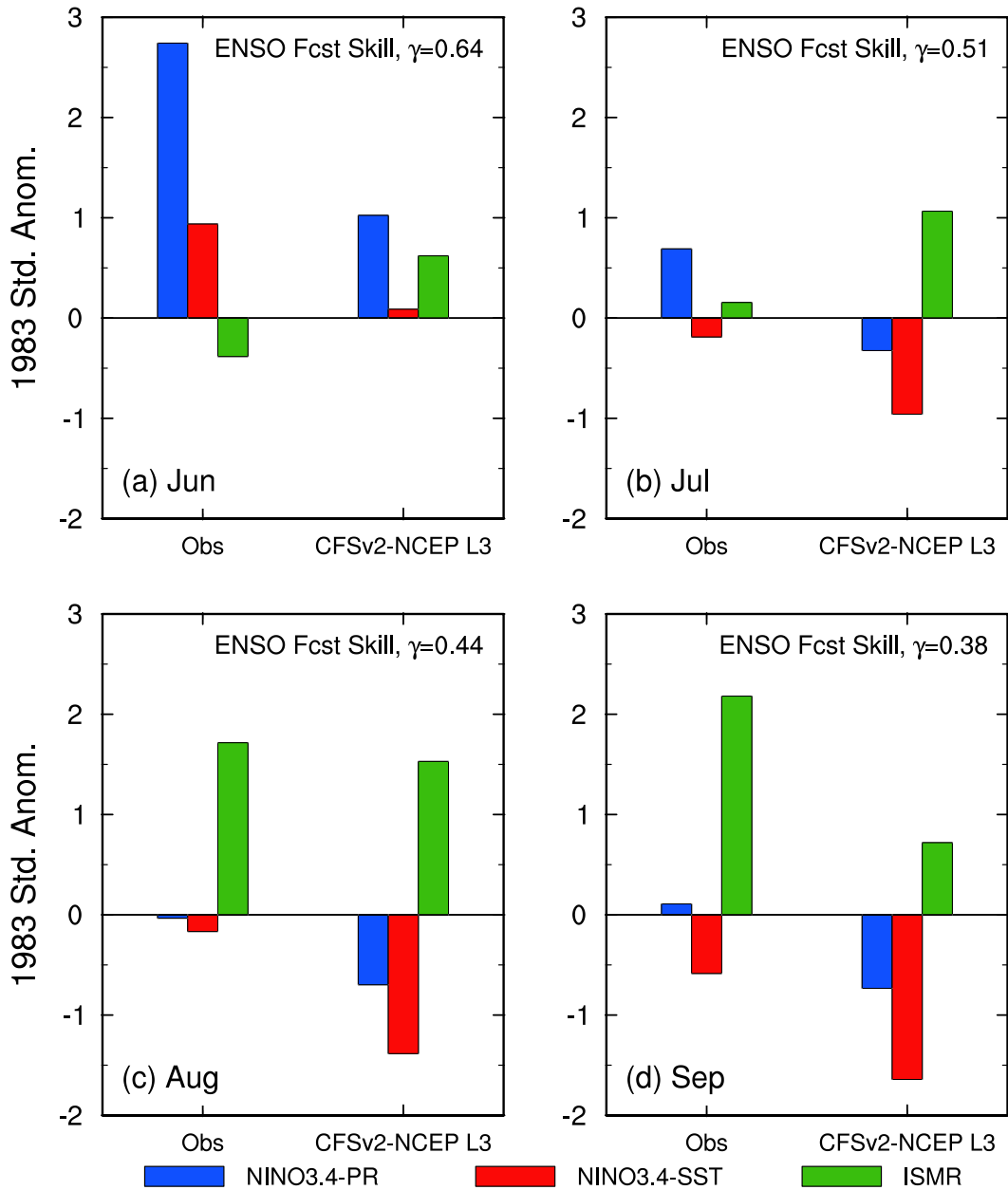


Figure 5: Monthly standardised anomalies of NINO3.4 rainfall (NINO3.4-PR) plotted along with the corresponding anomalies of ENSO index (NINO3.4-SST) and ISMR from observation and ensemble mean of CFSv2-NCEP L3 for a) June, b) July, c) August and d) September. Corresponding correlations ( $\gamma$ ) are also given.

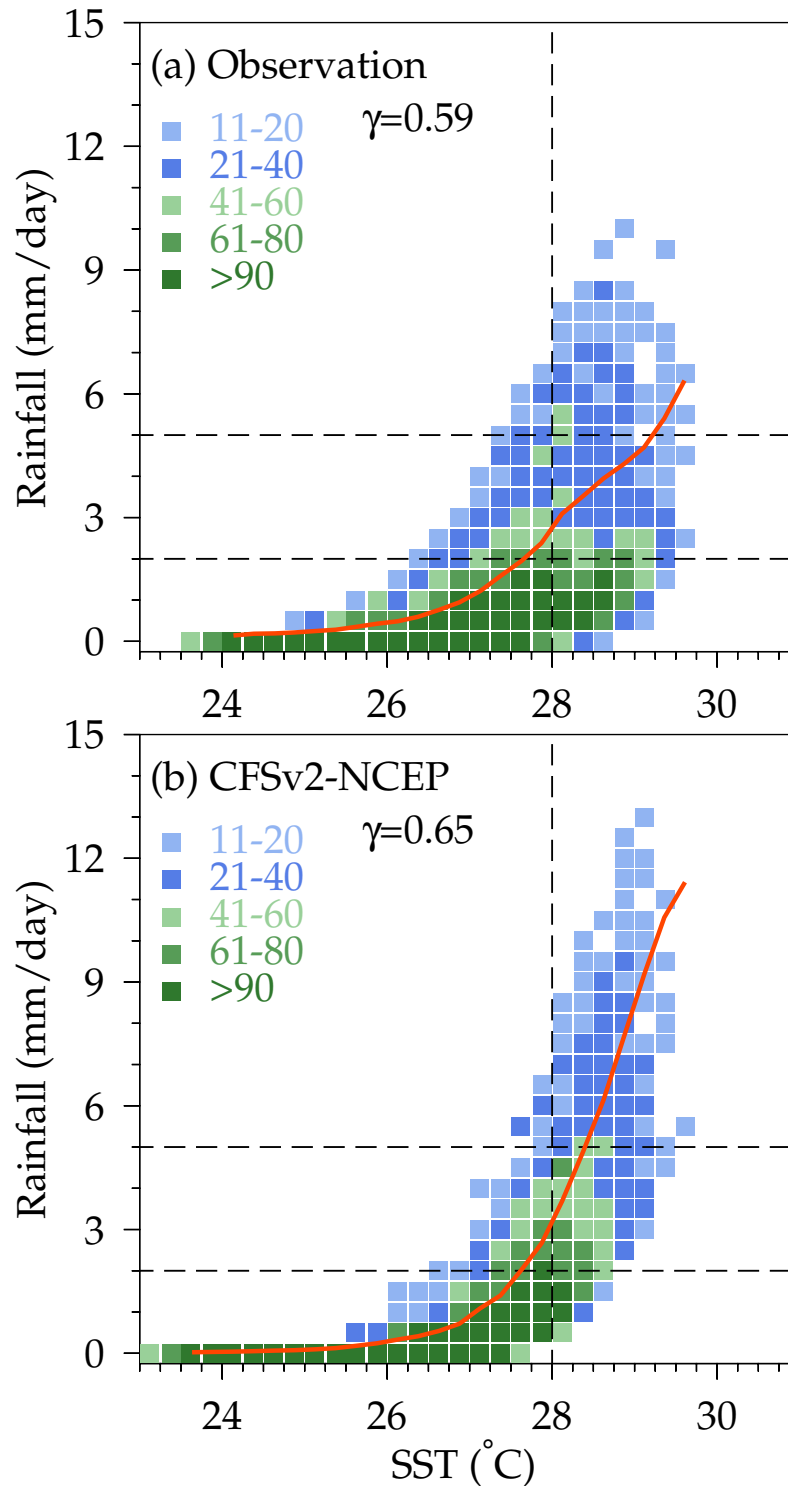


Figure 6: Distribution of the number of points for each 0.25°C SST and 0.5 mm/day rainfall bins along with the mean rainfall versus mean SST for each bin (red curve) showing the relationship between rainfall and SST, for June, July, August and September of 1982-2010 period over NINO3.4 in e) observation and f) ensemble mean of CFSv2-NCEP L3.

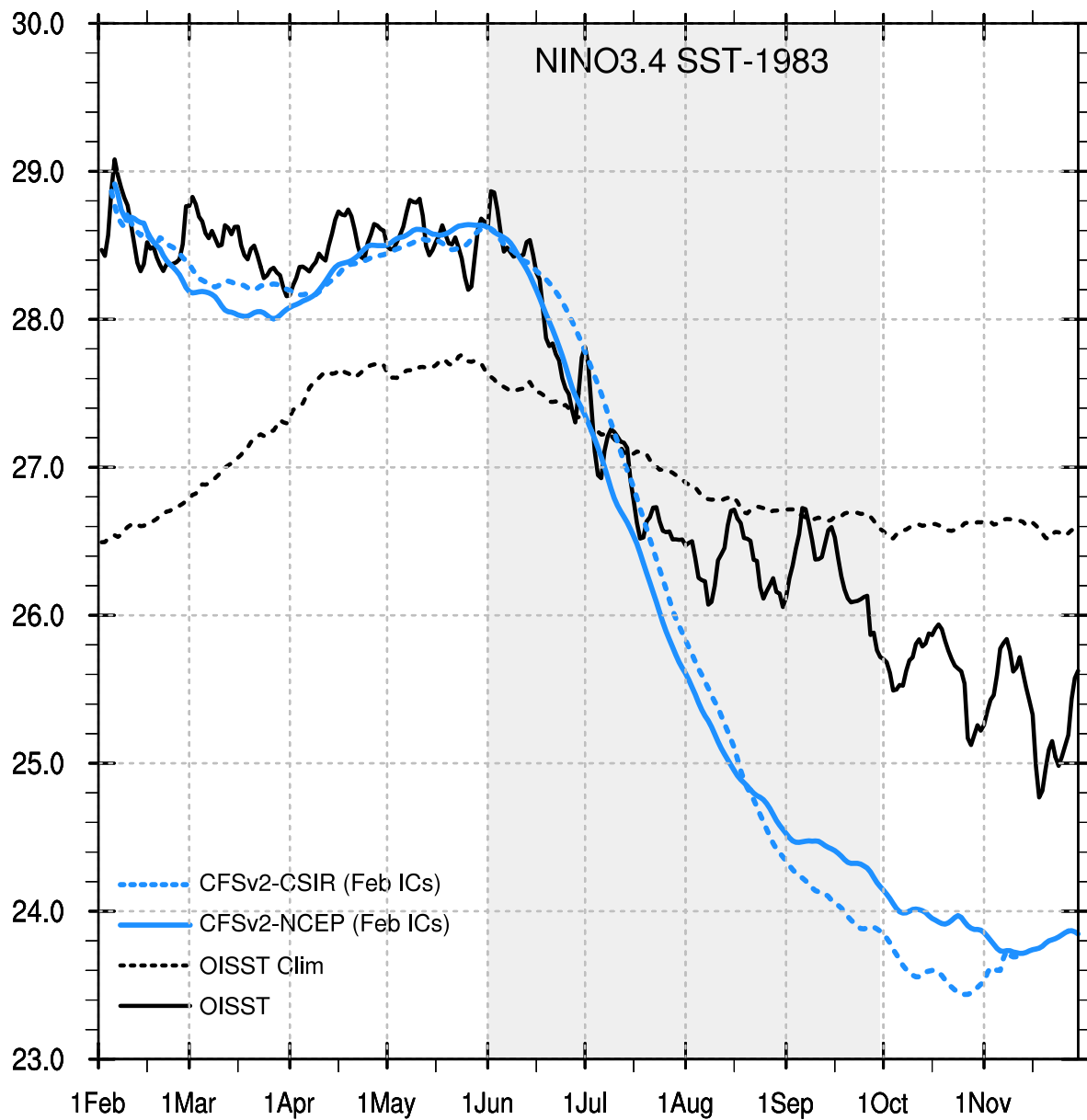


Figure 7: Evolution of daily SST averaged over NINO3.4 from OISST observation, OISST daily climatology and ensemble mean CFSv2-NCEP reforecasts with February (L3) initial conditions (ICs), and ensemble mean CFSv2-CSIR reforecasts (current version of CFSv2 being used in India) with February (L3) ICs.

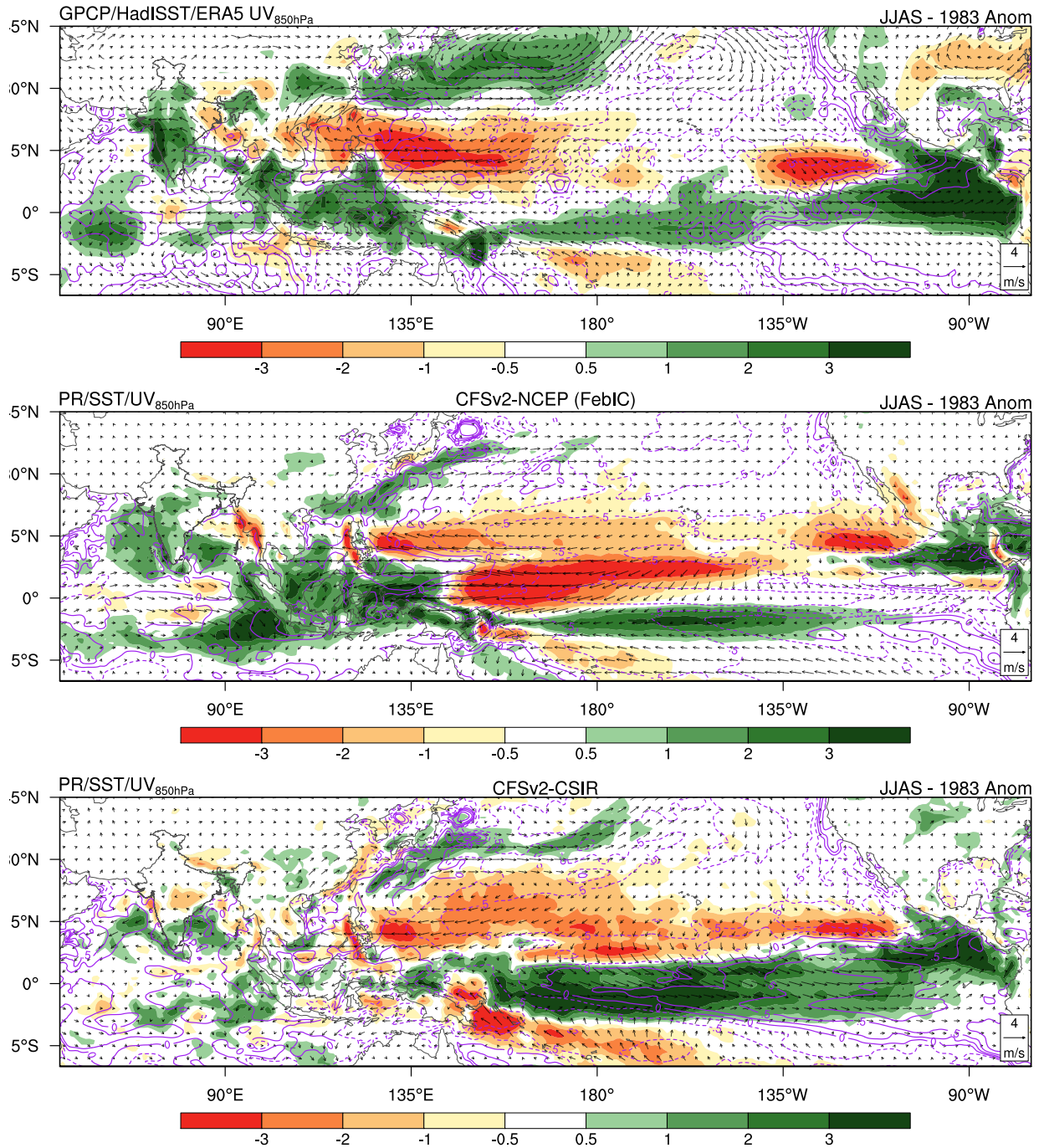


Figure 8: Seasonal summer mean (JJAS) anomalies of rainfall (shaded), SST (contour) and 850 hPa winds (vectors) from i) observation (top), and ensemble means of ii) CFSv2-NCEP reforecasts with L3 ICs (middle) and iii) CFSv2-CSIR reforecasts with 5 ICs (bottom).

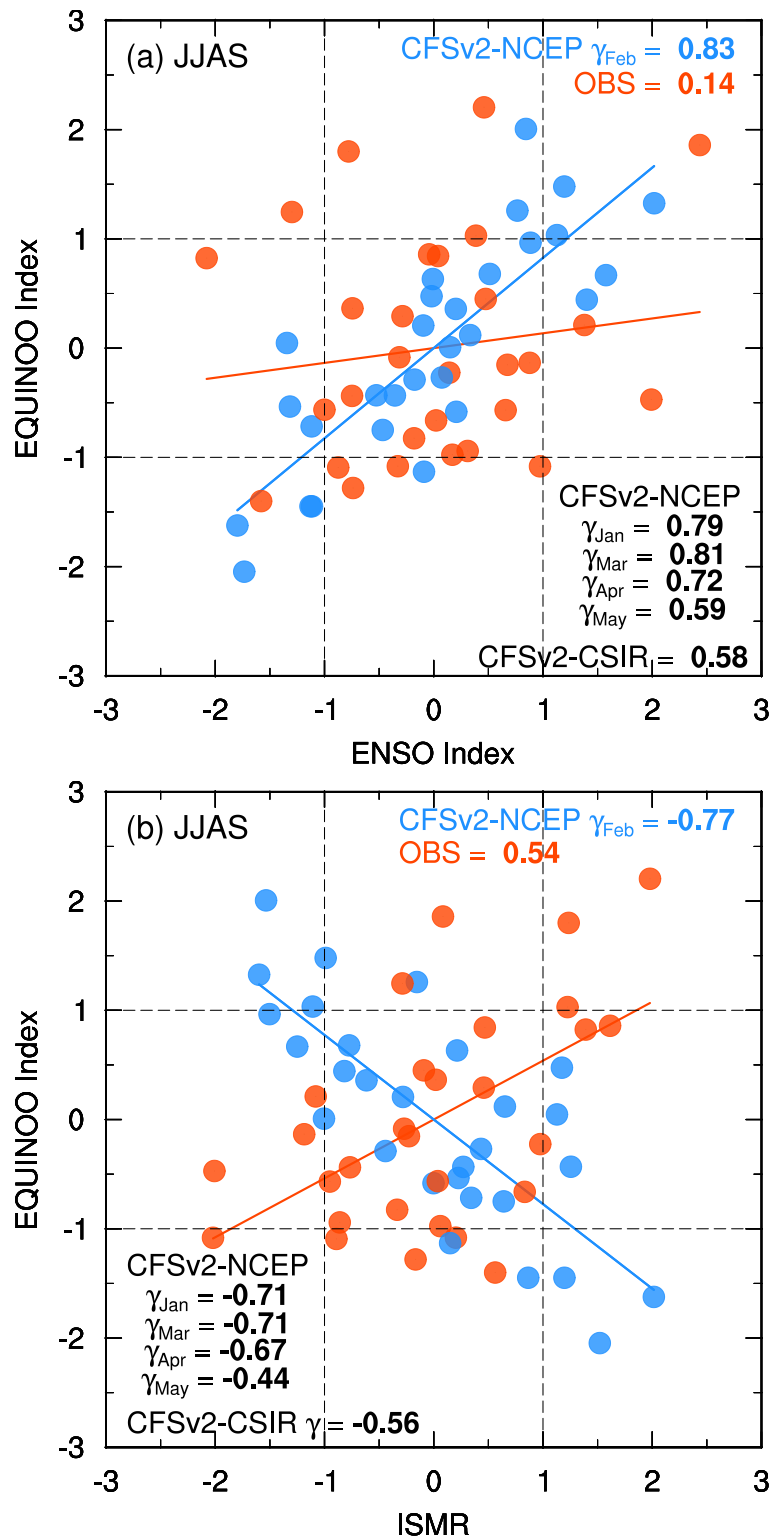


Figure 9: a) Anomalies of EQUINOO index plotted against ENSO index for CFSv2-NCEP L3 (blue) and observation (red). b) Anomalies of EQUINOO index plotted against ISMR for CFSv2-NCEP L3 (blue) and observation (red). Respective regression lines are drawn and correlations ( $\gamma$ ) for CFSv2-NCEP L4, L2, L1 and L0, and CFSv2-CSIR with late-April/early-May ICs, are given in bottom-left corner and for CFSv2-NCEP L3 and observation are given in top-right corner of a and b.